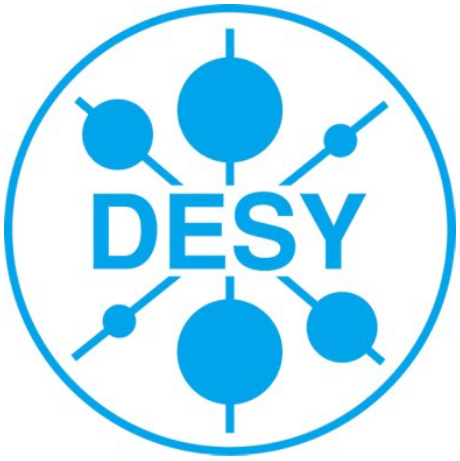

Coherence properties of P10 beamline at PETRA III performed by XRT software simulations.

Khubbutdinov Ruslan, NRNU MEPhI, Russia

10 September 2015

Supervisors:

Petr Skopintsev

Ilya Besedin

Prof. Dr. Ivan A. Vartanyants

Abstract

During the last several years new methods for structural analysis based on X-ray radiation interaction with matter such as XPCS, CXDI and others were developed. Significant part of them rely on powerful radiation sources with high coherent properties and high-brilliance of the beam. It is clear that understanding of those properties is of importance for the scientific community. Results of simulation ray tracing and wave propagation in X-ray regime for study coherence properties of P10 beamline at PETRA III synchrotron are presented in this research.

Contenst

I. Introduction

At present, a class of methods for structural analysis based on different physical processes of X-ray interaction with matter is being developed. The resulting structural information highly depends on the method applied. Applicability of methods directly depends on the task, so that many of them are complement to each other. Using a combination of methods with high spatial resolution for finding local structural components and low spatial resolution for macroscopic mutual arrangement leads to full determination of the structure. In case of local structure determination, high spatial resolution comes from short wavelengths on one hand and high coherence properties of probing waves on the other. That is why modern sources of highly-brilliant x-ray radiation begin to play an increasingly important role.

Storage rings are nowadays the principle sources of high-brilliance x-rays beams. They provide beams which are highly stable in photon energy, beam intensity, size and position. The photon energy is easily tunable over a wide spectrum. The most powerful sources, such as European XFEL, LCLS and FLASH, have the average brilliance above 10^21 ph/(s mm^2 mrad^2 %0.1 BW). Third generation x-ray sources typically have brightness of a few orders of magnitude lower, for example, PETRA III storage ring has 10^19 ph/(s mm^2 mrad^2 %0.1 BW). With the advent of highly brilliant x-ray sources, a new type of experiments became available, which utilize the high degree of coherence of x-ray beams. In lenseless imaging techniques, due to the fact that only the intensities are measured on the detector, phase retrieval methods are required to recover the missing phase and, consequently, the structure of the object. The examples of such novel methods where far-field diffraction pattern is recorded when coherent radiation illuminates the sample, include CXDI and x-ray ptychography [1].

In order to increase the amount of emitted radiation, arrangements of striped bending magnets, called wigglers and undulators, were created. Radiation generated by these insertion devices is confined to a narrow cone of angle $\Theta \sim 1/2\gamma$, where γ is the Lorentz factor [2]**.** The conversion from undulator radiation to wiggler radiation can be described by the undulator parameter K. For $K \leq 1$, undulator radiation with spectral harmonics is generated, for $K > 1$ wiggler radiation is produced. For instance, at PETRA III, the undulator parameter is K = 2.2 for P10 undulator radiation. The harmonics of the radiation can be described as dipole oscillations of the electron which propagates through the undulator, so that the frequency of emitted radiation in the frame moving with the electron is given by the frequency of oscillation. Typically, the radiation properties, such as brilliance and the degree of transverse coherence are determined by the electron bunch properties which are in turn defined by the accelerator ring characteristics. One of the most important characteristic is the electron beam emittance $\varepsilon_e = \sigma_e \sigma'_e$, where σ_e and σ'_e is the size of the electron bunch and its divergence, respectively. The low emittance of the electron bunch provides a low emittance ε of the photon beam and this leads to a higher brilliance and a higher coherent photon flux of the source. Usually, all storage rings have higher emittance in horizontal direction than in vertical.

The great majority of structural analysis methods require high coherence of the beam generated at x-ray sources and understanding of those properties is of crucial importance for the scientific community.

II. Theory

Mutual coherence function MCF

The basics of radiation coherence theory can be introduced by the following equations. The main role in describing the coherence phenomena, i.e. interference between the fields, is played by the mutual coherence function (MCF) [3]

$$\Gamma(r_1, r_2, t_1, t_2) = < E^*(r_1, t_1)E(r_2, t_2) >. \qquad (2.1)$$

This function describes correlations between two complex values of the electric field at different points r1 and r2 in space and at different times t1 and t2. The brackets <> denote the ensemble average. If two points and times coincide then MCF turns into average intensity

$$< I(r, t) > \; = \Gamma(r, r; t, t) = < |E(r, t)|^2 >. \qquad (2.2)$$

Normalization of MCF

$$\gamma(r_1, r_2, t_1, t_2) = \frac{\Gamma(r_1, r_2, t_1, t_2)}{\sqrt{<I(r_1, t_1)>}\sqrt{<I(r_2, t_2)>}} \qquad (2.3)$$

gives us the complex degree of coherence (CDC). This measure can often be determined experimentally as contrast of the interference fringes. For stationary and ergodic wave fields the MCF is invariant under time translation and thus can be written as

$$\Gamma(r_1, r_2; \tau) = < E^*(r_1, t\,)E(r_2, t + \tau) >_T, \qquad (2.4)$$

where $\tau = t_2 - t_1$, and ensemble average is replaced by the time average.

Cross-spectral density function CSD

The Fourier transform of MCF defines the cross-spectral density function (CSD)

$$W(r_1, r_2, \omega) = \int \Gamma(r_1, r_2, \tau)e^{-i\omega t}d\tau. \qquad (2.5)$$

The Fourier inverse equation is known as the generalized Wiener-Khintchine theorem

$$\Gamma(r_1, r_2, \tau) \; = \frac{1}{2\pi}\int W(r_1, r_2, \omega)e^{i\omega t}d\omega. \qquad (2.6)$$

When two points coincide, CSD represents the spectral density of the radiation field

$$S(r, \omega) = W(r, r; \omega). \qquad (2.7)$$

The original Wiener-Khintchine theorem for this case would give

$$\Gamma(r, r; \tau) = \frac{1}{2\pi}\int S(r, \omega)e^{i\omega t}d\omega. \qquad (2.8)$$

A convenient measure of spatial coherence is the normalized version of CSD

$$\mu(r_1, r_2, \omega) = \frac{W(r_1, r_2, \omega)}{\sqrt{S(r_1, \omega)}\sqrt{S(r_2, \omega)}}, \qquad (2.9)$$

which is called the spectral degree of coherence (SDC). For instance, the values of that function depending on slits separation r1 and r2, are determined in the classical Young's experiment. Another convenient measure of coherence, the degree of transverse coherence ζ, that characterizes coherence properties of a wave field by only single number, can be introduced as

$$\zeta(\omega) = \frac{\int |W(r_1, r_2, \omega)|^2 dr_1 dr_2}{(\int S(r, \omega) dr)^2}. \qquad (2.10)$$

According to that, the values of the parameter $\zeta(\omega)$ lie in the range of $0 \leq \zeta(\omega) \leq 1$ where $\zeta(\omega) = 1$ and $\zeta(\omega) = 0$ correspond to fully coherent and incoherent radiation, respectively.

Propagation of Correlation Functions

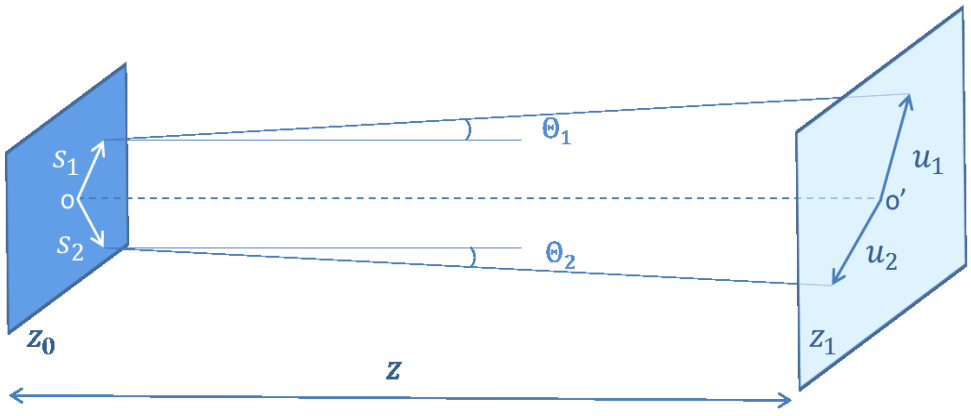

Fig. 1. The propagation geometry. The source is positioned at z_0 plane and is described by $W(s_1, s_2, \omega)$. CSD $W(u_1, u_2, \omega)$ of the radiation field in the observation plane positioned at distance z from the source is calculated (see Eq. (2.11)).

Propagation of correlation functions from the source plane at z0 to the plane at distance z from the source is governed by the following formula

$$W(u_1, u_2, z_1, \omega) = \iint W(u_1, u_2, z_0, \omega) P_z^*(u_1, s_1; \omega)\, P_z(u_1, s_1; \omega) ds_1 ds_2, \qquad (2.11)$$

where $W(s1, s2, z0; \omega)$ is SCD in the source plane z0, and $P_z(u, s; \omega)$ is the propagator. The integration is perfomed in the source plane (s_1, s_2). In the paraxial approximation valid for $kz(\frac{|u-s|}{z})^4 \ll 8\pi$, the propagator can be written as

$$\mathrm{P(u,\ s;\ \omega)} = \frac{k}{2\pi i}\frac{e^{ikz}}{z}\exp(ik\frac{|u-s|^2}{2z}). \qquad (2.12)$$

Propagation of SCD through a thin optical element can be described by transmission function $T(u, \omega)$

$$W(u1, u2, z, \omega) = W(u1, u2, z, \omega) T(u1, \omega) T(u2, \omega). \qquad (2.13)$$

Young's double slit experiment

Young's double slit experiment is the most common and direct method for characterization of coherence and for demonstrating the interference effect.

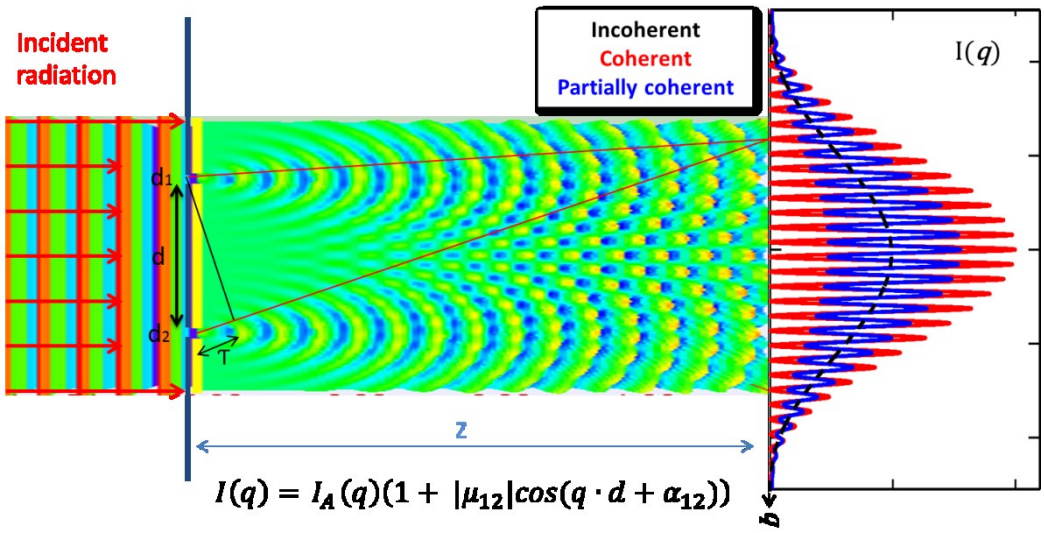

Fig. 2. Young's double slit experiment geometry

In Young's double slit experiment, partially coherent wave-field is incident on an opaque screen with two separated slits. If the field transmitted by different slits is correlated, then due to the wave superposition principle, the total radiation field in the observation plane will have interference fringes. If these fields are uncorrelated, then the intensities from the individual pinholes sum up and no interference is observed. To calculate the intensity distribution simulated in the double slit experiment, we start with the field incident on the aperture, which can be described by CSD $W(s_1, s_2, \omega)$. The CSD behind the double slit can be found by using equation (2.11) and the transmission function of a double slit

$$T(s) = T_1(s) + T_2(s). \qquad (2.14)$$

It can be shown [3], the simplified formula for the diffraction pattern can be written as

$$I(\boldsymbol{q}) = I_A(\boldsymbol{q})\big(1 + |\mu_{12}|cos(\boldsymbol{q} \cdot \boldsymbol{d} + \alpha_{12})\big), \qquad (2.15)$$

where $\boldsymbol{q} = \frac{kr}{z}$ is the transmitted pulse, $\boldsymbol{d}$ – separation between the slits, $I_A(\boldsymbol{q})$ is the intensity pattern produced by a single slit, α_{12}, the phase difference between the slits, and μ_{12} is SDC.

Let us now make three assumptions and derive the precise formulas for double slits diffraction pattern $I(\boldsymbol{q})$. First, let us assume that scattering at the slits occurs in the far-field. Second, let the slit sizes at plane (x, y) be so small that the phases φ_1, φ_2 and absolute values $A_1 = |E_1(x, y)|, A_2 = |E_2(x, y)|$ of the electric fields at the slits be constant. Also, let the slits be separated in vertical direction, so that vertical spatial coherence is analyzed in the double slits experiment.

Further, let a_x,a_y and D denote the horizontal, vertical dimensions of the slits, and separation between them, respectively, and let $\varphi_{12} = \varphi_2 - \varphi_1$ correspond to the phases difference between the fields in the slits. Finally, let us assume that z_1, z_2 are undulator-slits and slits-detector

distances, respectively, and λ is the wavelength of the undulator radiation. Then, in reciprocal space the intensity at the detector in Young's double slits experiment is

$$I(q_x, q_y) = E_1^2 + E_2^2 + 2E_1E_2|\mu_{12}|\cos[-q_y\mathrm{D} + \varphi_{12}], \qquad (2.16)$$

where

$$E_1 = E_1(q_x, q_y) = A_1 \cdot \frac{\sin\left(\frac{a_x q_y}{2} - \frac{ka_x\mathrm{D}}{2}\left(\frac{z_1+z_2}{z_1z_2}\right)\right)}{\frac{a_x q_y}{2} - \frac{ka_x\mathrm{D}}{2}\left(\frac{z_1+z_2}{z_1z_2}\right)} \cdot \frac{\sin\left(-\frac{a_y q_x}{2}\right)}{-\frac{a_y q_x}{2}}, \qquad (2.17)$$

$$E_2 = E_2(q_x, q_y) = A_2 \cdot \frac{\sin\left(\frac{a_x q_y}{2} + \frac{ka_x\mathrm{D}}{2}\left(\frac{z_1+z_2}{z_1z_2}\right)\right)}{\frac{a_x q_y}{2} + \frac{ka_x\mathrm{D}}{2}\left(\frac{z_1+z_2}{z_1z_2}\right)} \cdot \frac{\sin\left(-\frac{a_y q_x}{2}\right)}{-\frac{a_y q_x}{2}}, \qquad (2.18)$$

and

$$q_x = \frac{kx}{z_2},\ q_y = \frac{ky}{z_2},\ k = \frac{2\pi}{\lambda}. \qquad (2.19)$$

Formulas (2.16-2.19) would be further used in the "Results" section for fitting the simulation data and retrieving SDC $|\mu_{12}|$ for ranges of slits separations D.

Gaussian Schell-Model

A useful model to describe the radiation properties of partially coherent sources is the Gaussian Schell-model (GSM). The model was recently successfully applied to FEL and synchrotron radiation [4]. SCD of GSM source positioned at z_0 plane can be expressed as

$$W(s_1, s_2) = W(s_{1x}, s_{2x})W(s_{1y}, s_{2y}) \qquad (2.20)$$

where

$$W(s_{1x}, s_{2x}) = \sqrt{S_0}\exp\left(-\frac{s_{1x}^2 + s_{2x}^2}{4\sigma_x^2} - \frac{(s_{2x} - s_{1x})^2}{2\xi_x^2}\right) \qquad (2.21)$$

Here S_0 - normalization constant, and the parameters $\sigma_{x,y}$ and $\xi_{x,y}$ define the source size and transverse coherence length in the source plane in x- and y-directions, respectively. In this equation the frequency dependence omitted, and GSM applied to narrowband radiation, where ω is average frequency.

In the frame of GSM, the degree of transverse coherence (2.10) factorizes into x and y components $\zeta = \zeta_x\zeta_y$. For each transverse direction, an analytical expression for ζ can be found

$$\zeta = \left(1 + \left(\frac{2\sigma}{\xi}\right)^2\right)^{-\frac{1}{2}} \qquad (2.22)$$

III. Synchrotron radiation from 3rd generation sources

Source properties

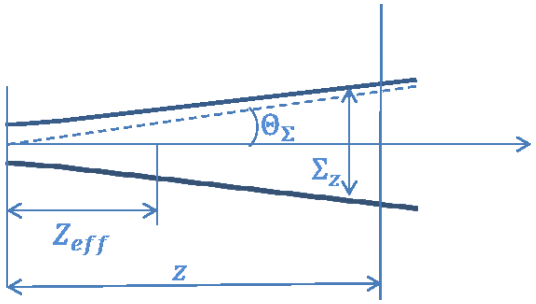

Fig. 3. Schematic illustration of the main parameters of Gaussian Schell-model source.

Source size and angular divergence of the single electron wavefield can be described by the following expressions

$$\sigma_r = \sqrt{2\lambda \frac{L_u}{4\pi}}, \qquad (3.1) \qquad \sigma_r' = \sqrt{\frac{\lambda}{2L_u}}. \qquad (3.2)$$

Electron bunch size and divergence can be calculated from the values of the electron bunch emittance $\mathcal{E}_{ex,y}$ and β-function of the synchrotron source [5]

$$\sigma_{ex,ey} = \sqrt{\mathcal{E}_{ex,y}\beta_{x,y}}, \qquad (3.3) \qquad \sigma'_{ex,ey} = \sqrt{\mathcal{E}_{ex,y}/\beta_{x,y}}. \qquad (3.4)$$

If $\sigma_{ex,ey}/\sigma_r \approx 1$ and $\sigma'_{ex,ey}/\sigma'_r \approx 1$, GSM can be used, and thus the photon source size and divergence are determined from the convolution of the size and divergence of the electron bunch (σ_e, σ_e') with the intrinsic radiation characteristics of a single electron (σ_r, σ_r')

$$\sigma_{x,y} = \sqrt{{\sigma_{ex,ey}}^2 + {\sigma_r}^2}, \qquad (3.5) \qquad \sigma'_{x,y} = \sqrt{{\sigma'_{ex,ey}}^2 + {\sigma'_r}^2}. \qquad (3.6)$$

Coherence length and beam size in the source plane are

$$\xi_{x,y} = \frac{\sigma_r \sigma_r'}{\sigma_{x,y}\sigma'_{x,y}}, \qquad (3.7) \qquad \Sigma(z) = \Delta(z) * \sigma, \qquad (3.8)$$

where $\Delta(z)$ is magnification factor

$$\Delta(z) = (1 + (\frac{z}{z_{eff}})^2)^{\frac{1}{2}}. \qquad (3.9)$$

Effective distance equivalent to Rayleigh distance for a fully coherent Gaussian beam is

$$Z_{eff} = 2\mathrm{k}\sigma^2\xi. \qquad (3.10)$$

Degree of transverse coherence can be calculated using equation (2.22). Coherence length (root mean square of SDC) at distance z is thus

$$\Xi(z) = \Delta(z) * \xi. \qquad (3.11)$$

XRT software

XRay Tracer package (xrt) is a python software library for ray tracing and wave propagation in x-ray regime. It is primarily meant for modeling synchrotron sources, beamlines and beamline elements (optical elements, apertures, screens) [6].

For scripting in python you need to prepare a script that gives instructions on how to get the wanted ray properties and prepare the graphs. The scripting is different for different backends (backend is a module or an external program that supplies ray distributions). Currently, xrt supports two backends: raycing – an internal backend – and shadow.

The main features of XRT are listed below:

- Publication quality graphics. 1D and 2D position histograms are simultaneously coded by hue and brightness. Typically, colors represent energy and brightness represents beam intensity. The user may select other quantities to be encoded by colors: angular and positional distributions, various polarization properties, beam categories, number of reflections, incidence angle etc. Brightness can also encode partial flux for a selected polarization and incident or absorbed power.
- Rays and waves. Classical ray tracing and wave propagation via Kirchhoff integral.
- Unlimited number of rays.
- Scripting in Python. Xrt can be run within Python scripts to generate a series of images under changing geometrical or physical parameters.
- Synchrotron sources. Bending magnet, wiggler, undulator and elliptic undulator are calculated internally within xrt.
- Energy dispersive elements. Implemented are gratings (also with efficiency calculations), Fresnel zone plates, Bragg-Fresnel optics. Crystals can work in Bragg or Laue cases, in reflection or in transmission.
- Global coordinate system. The optical elements are positioned in a global coordinate system. This is convenient for modeling a real synchrotron beamline. The coordinates in this system can be directly taken from a CAD library. The optical surfaces are defined in local systems for the user's convenience.
- Beam categories. xrt discriminates rays by several categories: good, out, over and dead. This distinction simplifies the adjustment of entrance and exit slits. An alarm is triggered if the fraction of dead rays exceeds a specified level.
- Parallel execution. xrt can be run in parallel in several threads or processes (can be opted), which accelerates the execution on multi-core computers. It can run on an external server (supercomputer), also without X window system (X11) support.

XRT simulations were done for P10 beamline at PETRA III synchrotron radiation source (see Fig. 4.). The beamline serves three main experimental goals:

- Investigation of sample dynamics in the range from microseconds to seconds by X-ray Photon Correlation Spectroscopy (XPCS).

- Coherent diffractive imaging of micro- and nanostructures (CDI).

- Time-resolved SAXS studies of complex liquids (Rheo-SAXS).

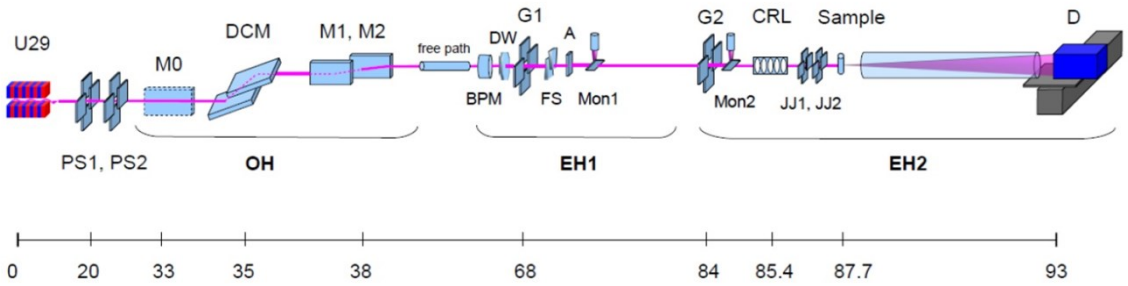

Fig. 4. P10 layout geometry, situated in sector 7 of PETRA III and a 5m long U29 undulator is installed in the straight section in low beta configuration. The beamline operates in the medium-hard X-ray regime (5-25keV).

Simple geometry of beamline was applied to simulate X-ray propagation and to study coherence properties of radiation source (see Fig.5)

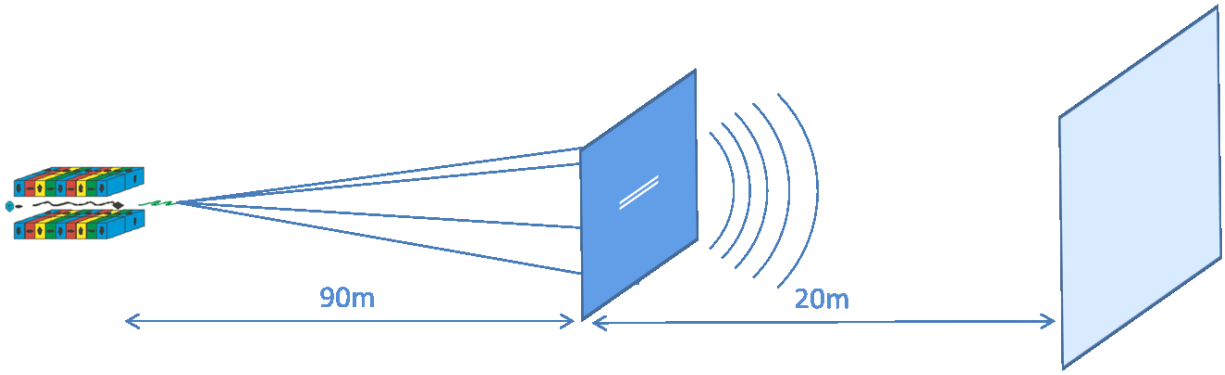

Fig. 5. Double slit geometry of PETRA III P10 beamline experiment (no optics) simulation performed with XRT. Schematic layout includes undulator, double slits and detector at 90m and 110 m position respectively.

XRT program works simulates the following sources of X-ray radiation: bending magnet, wiggler and undulator. The radiation emanating from the sources is further propagated either in rays or waves regime.

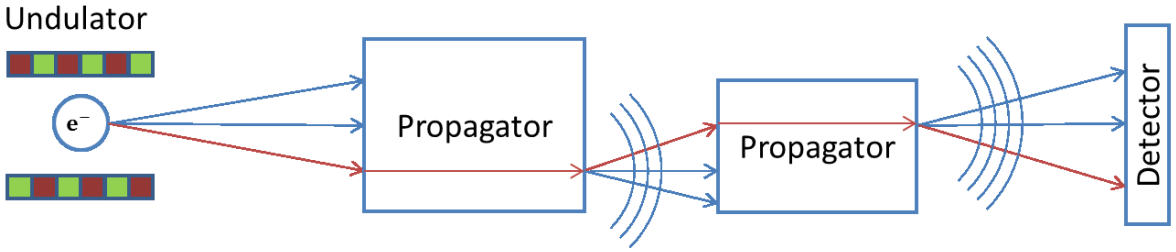

Fig. 6. Schematic of rays propagation.

In the ray regime, each single electron from the undulator source generates defined amount of rays, which spreads in angular vertical and horizontal directions also defined by user. Every time the program generates random grid on one of the chosen elements with desirable amount of points, and then electron generates the same amount of photons for further propagation through the apertures or optical elements (see Fig. 6). After spreading through the grid, new rays are generated reaching the next grid with uniform sampling on the detector. In this way, all rays spread through the beamline and reach the detector where they are summed for each point on the grid by amplitude and phase coherently for one electron and by intensity for desired amount of them.

IV. Results

Double slit simulation

All simulations for P10 beamline at PETRA III were made with the following parameters

P10 (PETRA III) characteristics	**XRT parameter**	**Value**
horizontal emittance	eEpsilonX ($\mathcal{E}_x$)	1 nm rad
vertical emittance	eEpsilonZ ($\mathcal{E}_y$)	0.01 nm rad
Undulator characteristics		
horizontal beta	betaX (β_x)	1.20
vertical beta	betaZ (β_y)	3.95
radiation energy	E0	12000 eV
undulator period	period	29 mm
number of periods	N	172
energy spread	eEspread	0-0.001
Electron characteristics		
energy	eE	6.08 GeV
current	eI	0.1 mA
number of electrons	nrep	200
Ray characteristics		
Amount of rays	mynrays	2*10^6 (2e6)
Minimum photon energy:	eMinRays	E0 - 0.4 eV
Maximum photon energy:	eMaxRays	E0 + 0.4 eV
Slits characteristics		
slits position	R0	90000 mm
Slits width	slitDx	1.5 mm
Slits height	slitDz	0.005 mm
Detector characteristics		
Detector position	dR	20 m
Size of the detector (x direction)	SCRx	1.5 mm
Size of the detector (y direction)	SCRz	1 mm
Bins in horizontal direction	xBins	512
Bins in horizontal direction	zBins	512
Bins per pixel (x direction)	xppb	1
Bins per pixel (y direction)	zppb	1

Here below the results of XRT simulations lie. For each slit separation from 40 µm to 400 µm the complex degree of coherence (CDC) functions were calculated by fitting in an 11 pixels cross-section of the interference pattern with analytic expression (eq. 2.16) (see Fig. 8, 9). To estimate the spatial coherence length, the values of the modulus of CDC were approximated by Gaussian function (see Fig. 10). The obtained coherence length from the vertical double slit simulation is 238 µm. All Young's double slit simulations were done for zero energy spread.

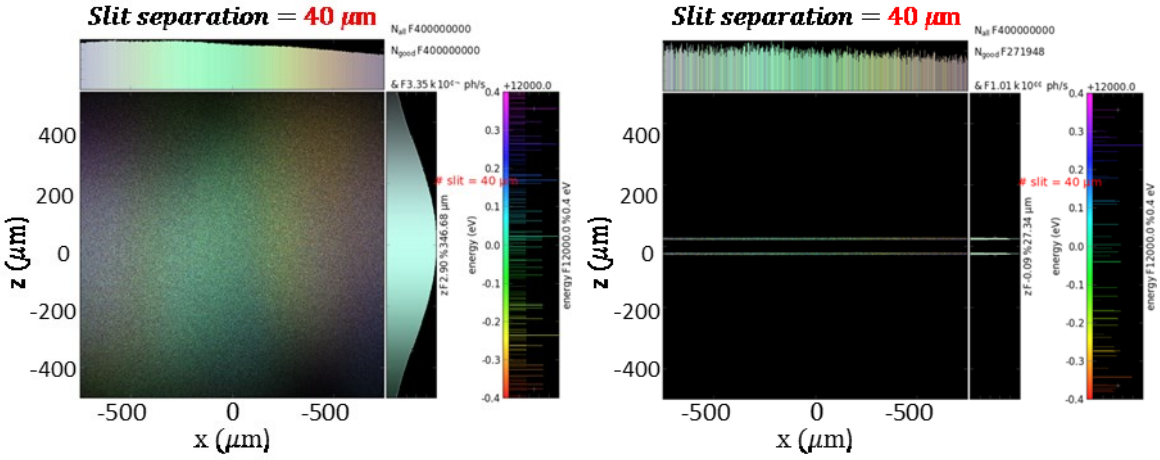

Fig. 7. a) Incident intensity at slits position 90 m. Each color determines the photon energy. Energy bandwidth is 0.8 eV. b) Intensity after double slits at 90m. Separation between the slits and slit widths are 40 µm and 5 µm, respectively.

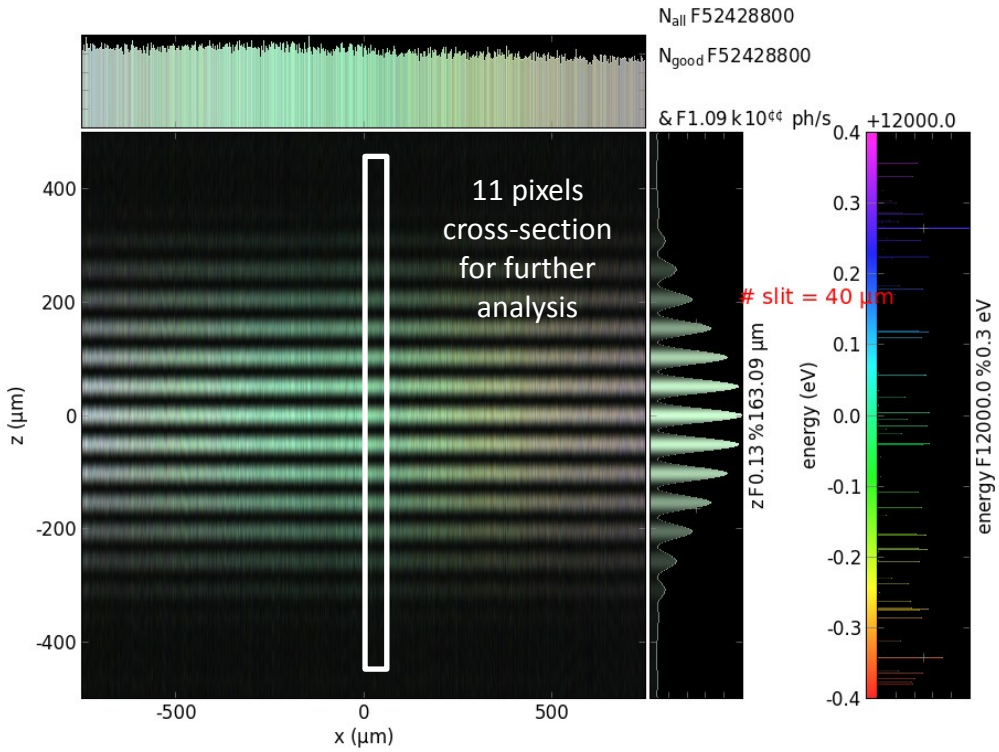

Fig. 8. Simulated double-slit interference patterns intensity for vertical slit separation of 50 µm at wavelength of 0.103 nm. White rectangle determines 11 pixels cross-section of interference patterns for further analysis.

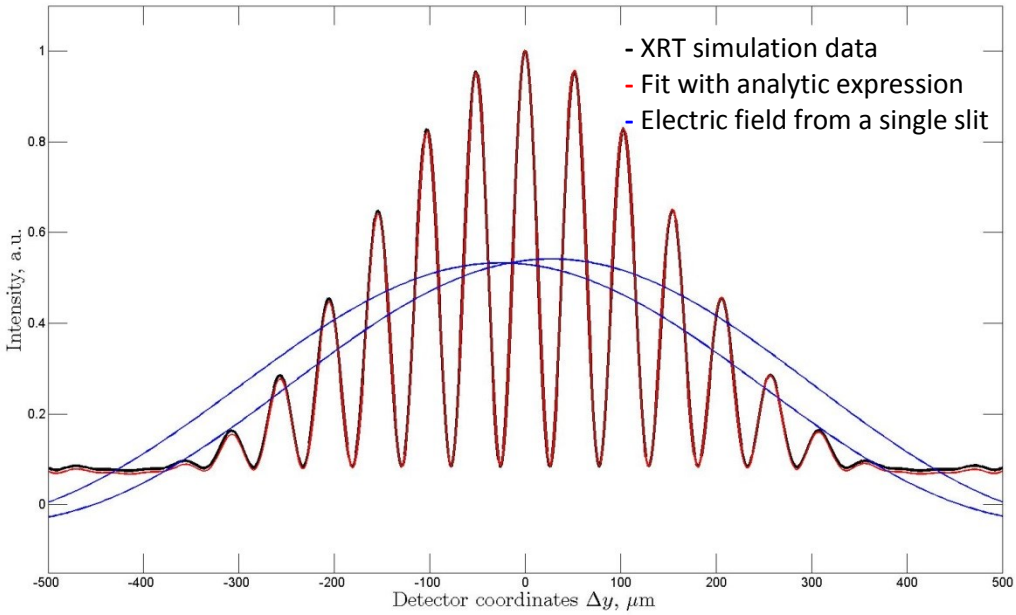

Fig. 9. Fit with analytic expression the results of interference patterns for double slit simulation. Black line corresponds to XRT simulation data, red and blue for analytic expression and electric field from a single slit, respectively.

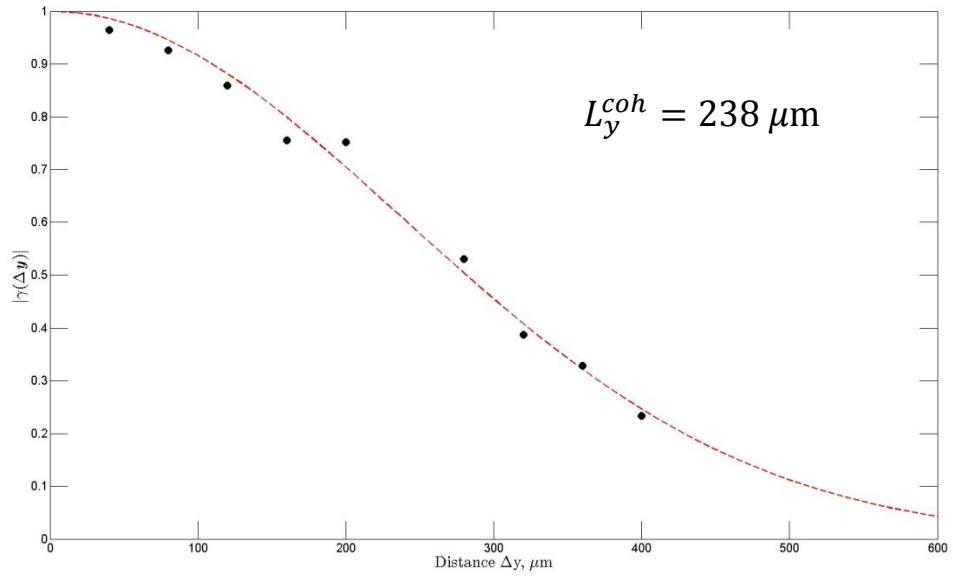

Fig. 10. Gauss approximation for double slit experiment in vertical direction. Degree of coherence and separations between slits performed on Y and X axis respectively.

Direct simulations of CSD

Second approach for characterization of spatial coherence by XRT simulations is the simulation of cross-spectral density function in vertical and horizontal directions. This method allows characterization of coherence properties directly. The schematic of simulation is similar to the double slit experiment, however, no apertures or optical elements were used. Generated x-rays from single electrons were propagated directly from the undulator to the screen.

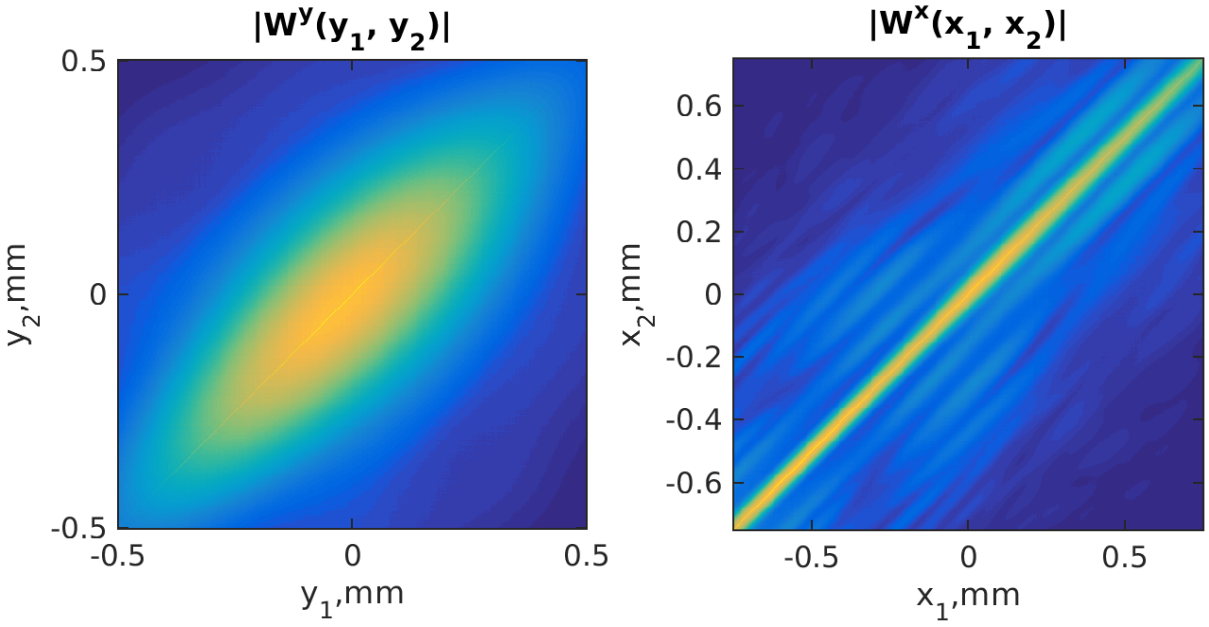

Fig. 11. Simulation of a) cross-spectral density function $W(y_1, y_2)$ in vertical direction at 90 m from the source and b) $W(x_1, x_2)$ in horizontal direction.

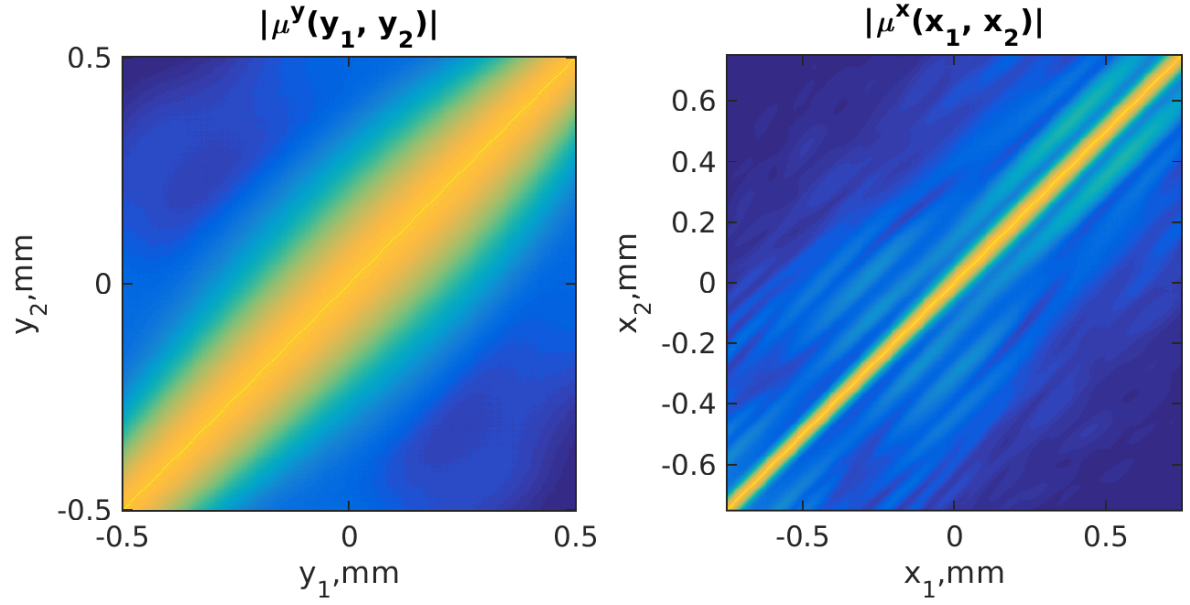

Fig. 12. Simulation of a) spectral degree of coherence function $\mu(y_1, y_2)$ in vertical direction at 90 m from the source and b) $\mu(x_1, x_2)$ in horizontal direction.

To calculate coherence properties of the source, spectral degree of coherence (SDC) functions were derived by dividing CSD $W(r_1, r_2)$ by spectral density $S(r, \omega)$ (see Figs. 12 a, b). Gaussian

approximation for diagonal cross section of SDC allows retrieving coherence length in vertical and horizontal directions (see Figs. 13, 14, 15). Using size of the beam and the coherence length, a degree of transverse coherence in vertical direction was obtained ζ = 0.35.

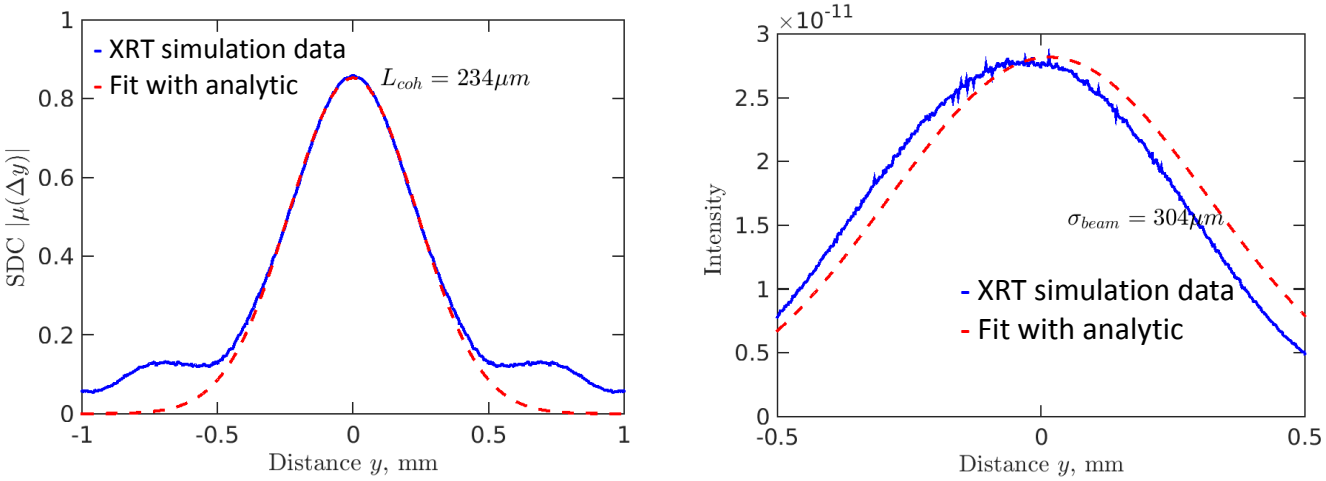

Fig. 13. Gaussian approximation for a) diagonal cross-section of SDC in vertical direction, blue and red line represent XRT simulation data and approximation, respectively, b) beam intensity.

Almost the same results were obtained for the simulation with energy spread, where ζ = 0.21.

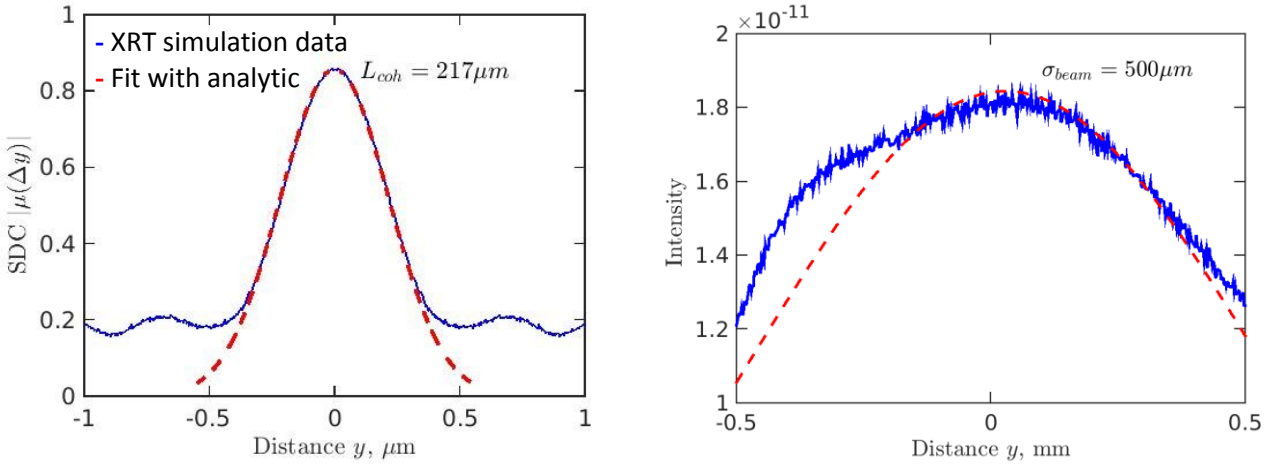

Fig. 14. Gaussian approximation for a) diagonal cross-section of SDC in vertical direction, blue and red line represent XRT simulation data and approximation, respectively, b) beam intensity.

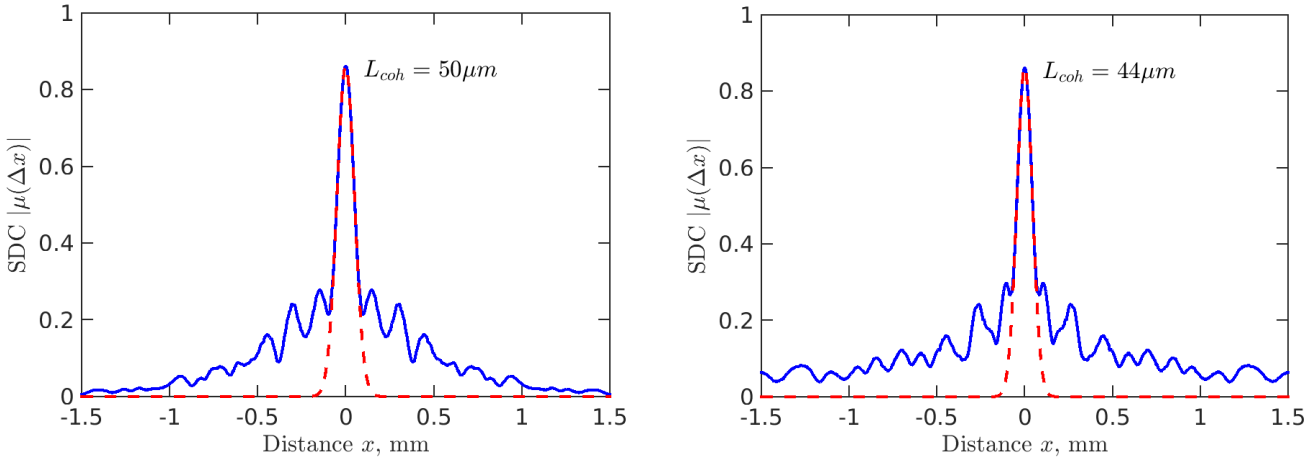

Fig. 15. Gaussian approximation for diagonal cross-section of SDC in horizontal direction for simulations a) without and b) with energy spread.

In comparing both approaches: the double slits experiment and direct retrieval of coherence from CSD and results obtained from Gaussian-Schell Model [7], we might say that they give similar results, which can be included in good error of calculation (see Fig.15). Coherence length gained from the double slit simulation and CSD simulation is about 238 µm and 234 µm, respectively, and result from Gaussian-Schell Model is 260 µm.

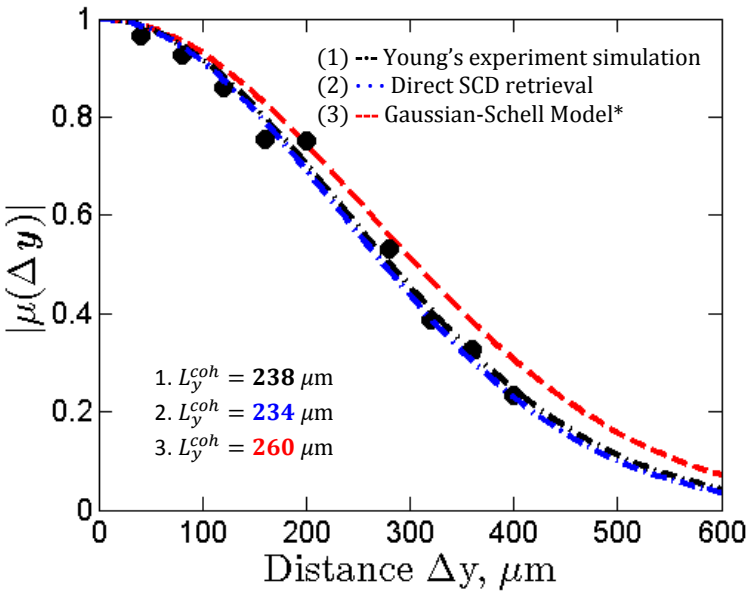

Fig. 15 Gauss approximations for double slit simulations (black line), diagonal cross-section of SDC simulations (blue line) in vertical direction and Gaussian-Schell Model prediction (red line).

The blue curve (Fig.15) has been normalized to exclude influence of noise. Due to the fact of low electron statistics and influence of noise both simulated results are not completely coinciding.

V. Conclusion and outlook

In summary, it was demonstrated how XRT software can be applied to the analysis of coherence properties of new generation x-rays radiation sources. It was shown how such essential values as coherence length and degree of coherence can be obtained from XRT simulations and can be used for understanding of coherence-based experiments. An important part of this research was devoted to showing that both methods give comparable results. Moreover, given the fact that XRT well reproduces theoretical estimates [4], it can be concluded that XRT well reproduces coherent properties of P10 beamline of PETRA III synchrotron x-ray radiation and can be used to simulate coherence-based experiments, including different types of radiation sources and beamline optics.

VI. References

[1] M. Rose *et al.*, *J. Synchrotron Rad.* 22, 819-827 (2015).

[2] D. Attwood. *Soft X-Rays and Extreme Ultraviolet Radiation*. Cambridge University Press, 1st edition (1999).

[3] J. W. Goodman. *Statistical Optics*. Wiley, New York (1985).

[4] 4. A. Singer. *Coherence properties of third and fourth generation x-ray sources. Theory and experiment*. Dissertation, Hamburg university, Germany. (2012).

[5] 5. K. Balewski *et al. PETRA III: A Low Emittance Synchrotron Radiation Source.* Technical report, DESY, Hamburg, Germany (2004).

[6] https://pypi.python.org/pypi/xrt.

VII. Appendix

Simulated double-slit interference patterns intensity for vertical slit separation and fit with analytic expression the results of interference patterns for double slit simulation. Black line corresponds to XRT simulation data, red and blue for analytic expression and electric field from a single slit, respectively.

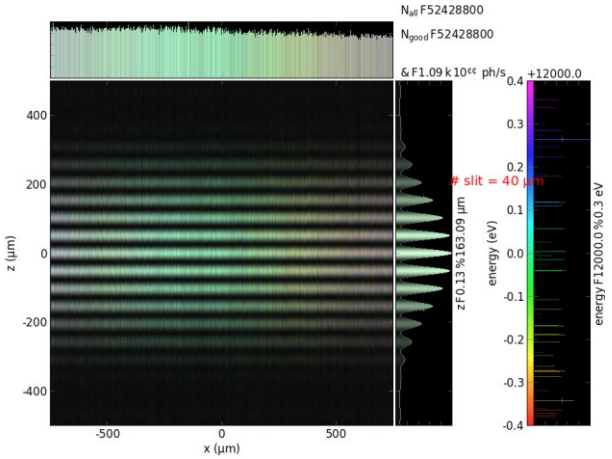

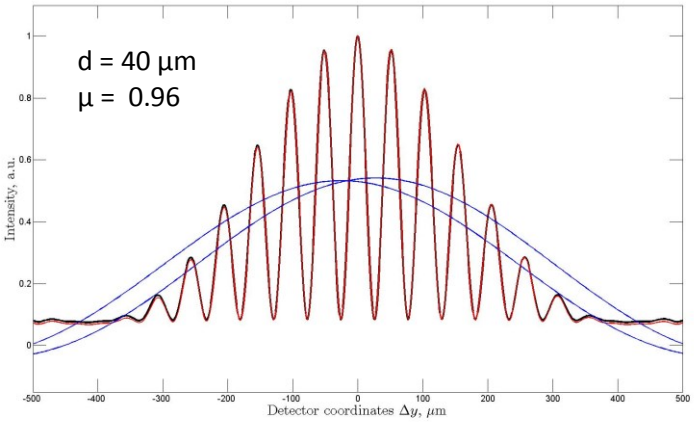

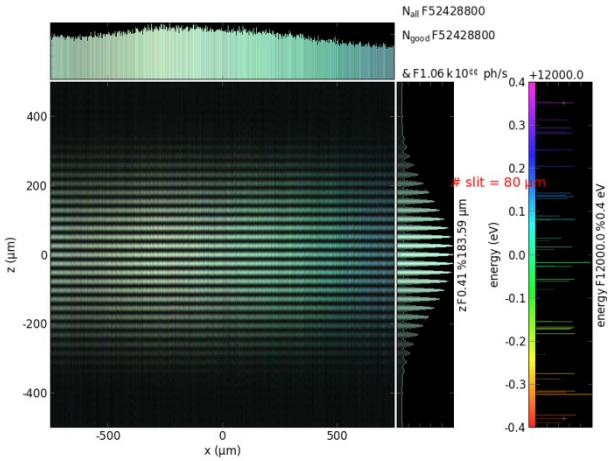

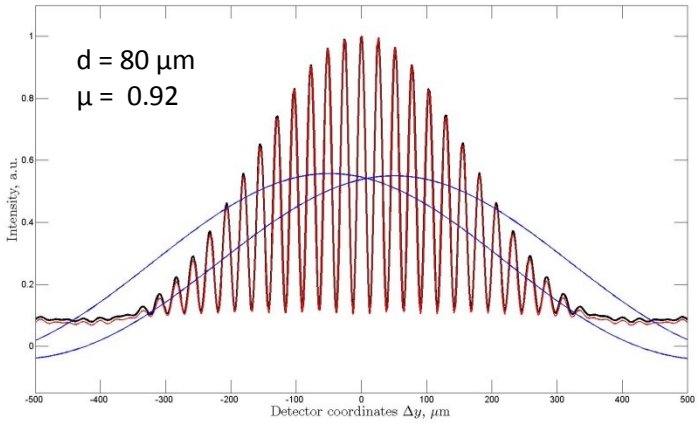

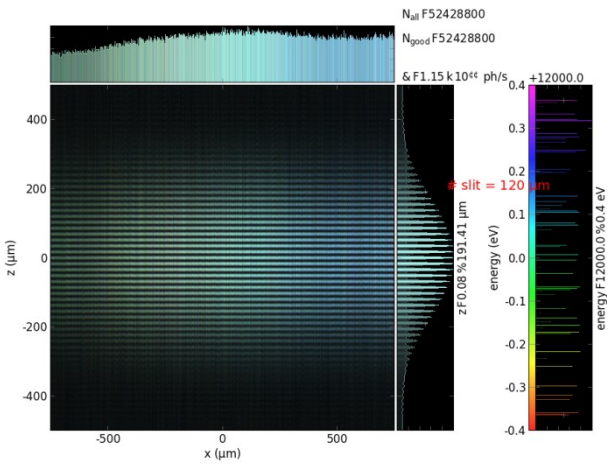

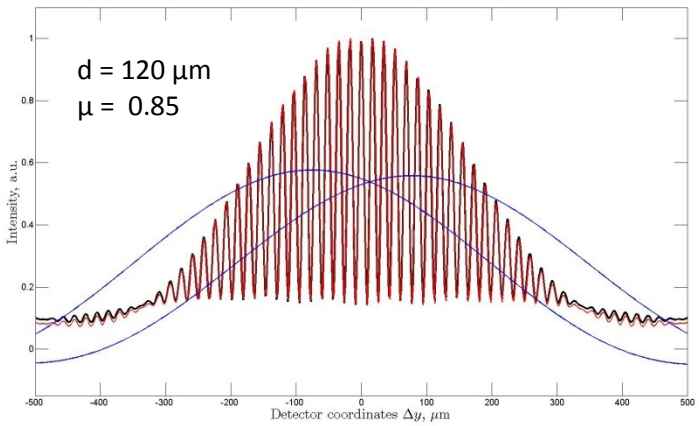

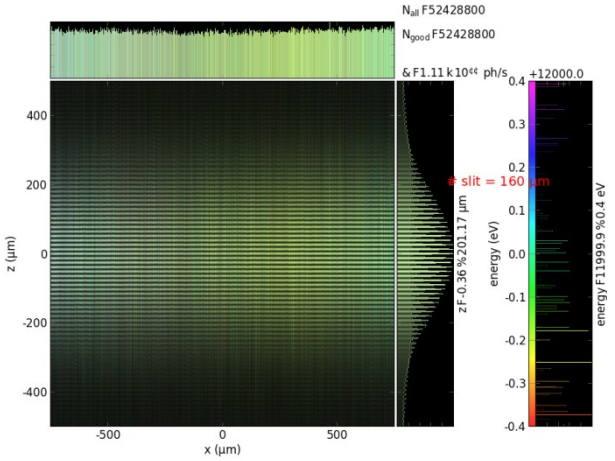
N_all F52428800
N_good F52428800
& F1.11 k 10^66 ph/s
+12000.0
slit = 160 µm
z F-0.36 %201.17 µm
energy (eV)
energy F11999.9 %0.4 eV
z (µm)
x (µm)

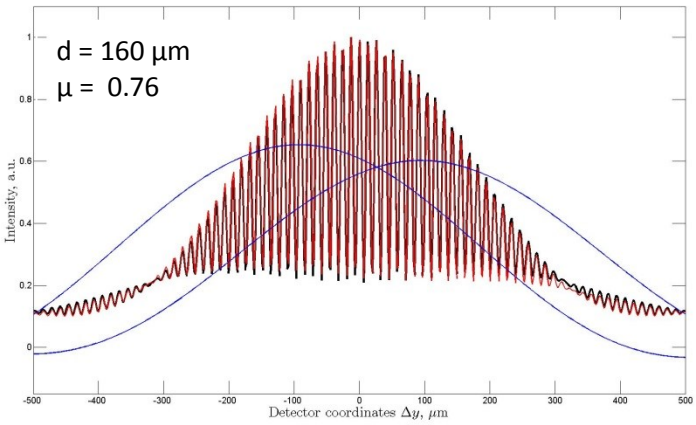
d = 160 µm
µ = 0.76
Intensity, a.u.
Detector coordinates Δy, µm

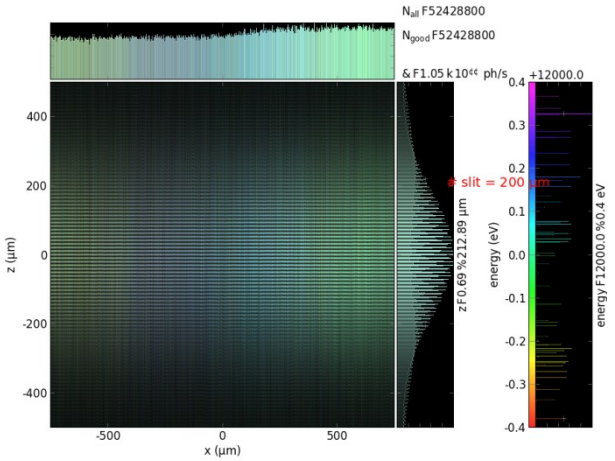
N_all F52428800
N_good F52428800
& F1.05 k 10^66 ph/s
+12000.0
slit = 200 µm
z F0.69 %212.89 µm
energy (eV)
energy F12000.0 %0.4 eV
z (µm)
x (µm)

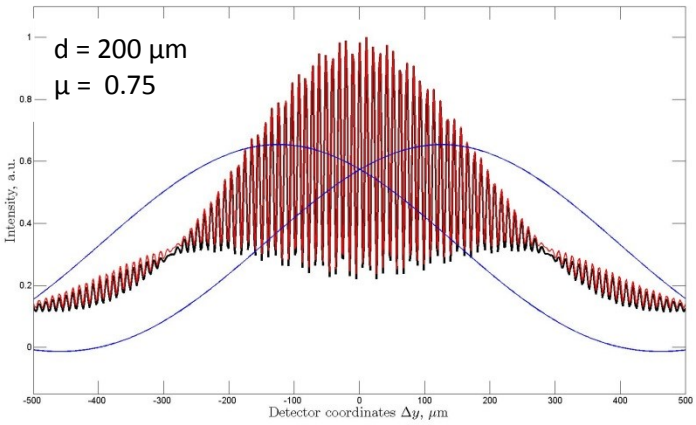
d = 200 µm
µ = 0.75
Intensity, a.u.
Detector coordinates Δy, µm

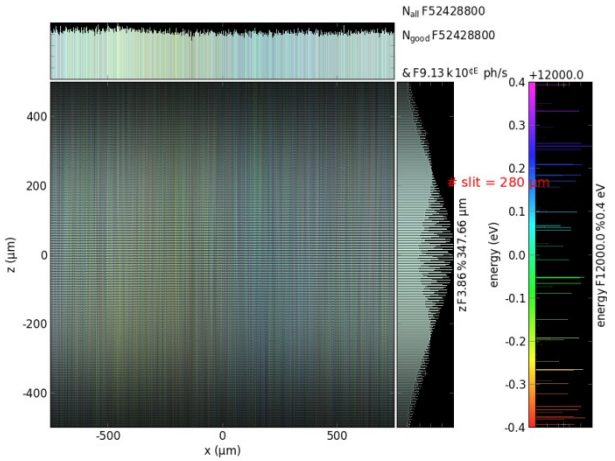
N_all F52428800
N_good F52428800
& F9.13 k 10^66 ph/s
+12000.0
slit = 280 µm
z F3.86 %347.66 µm
energy (eV)
energy F12000.0 %0.4 eV
z (µm)
x (µm)

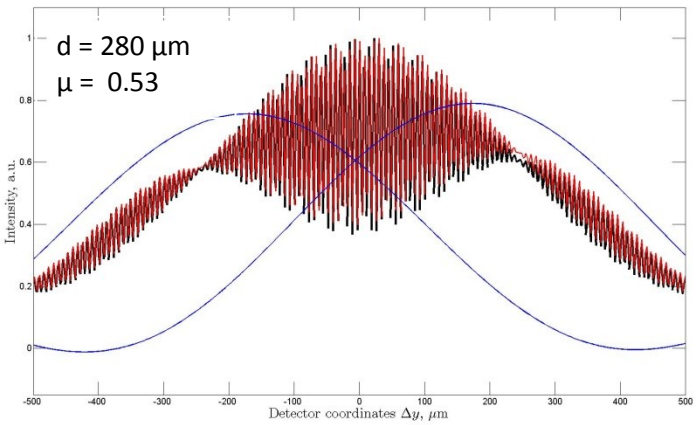
d = 280 µm
µ = 0.53
Intensity, a.u.
Detector coordinates Δy, µm

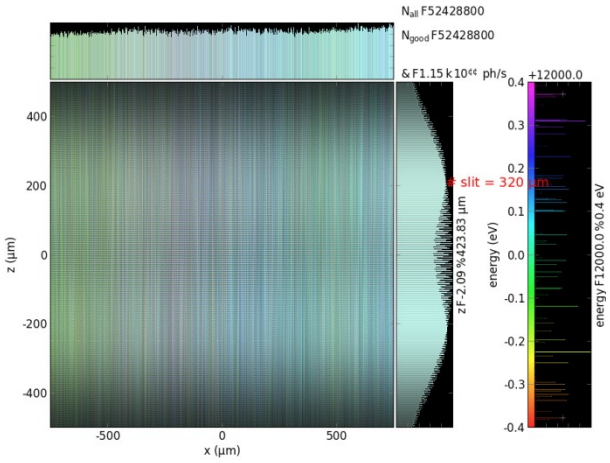
N_all F52428800
N_good F52428800
& F1.15 k10^6 ph/s
+12000.0
slit = 320 µm
z F-2.09 %423.83 µm
energy (eV)
energy F12000.0 %0.4 eV
z (µm)
x (µm)

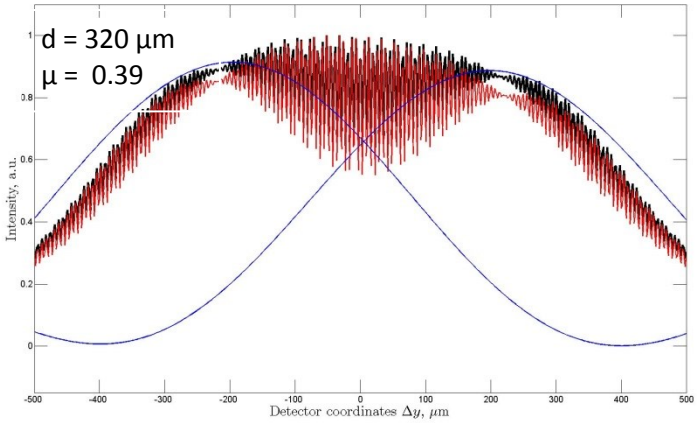
d = 320 µm
µ = 0.39
Intensity, a.u.
Detector coordinates Δy, µm

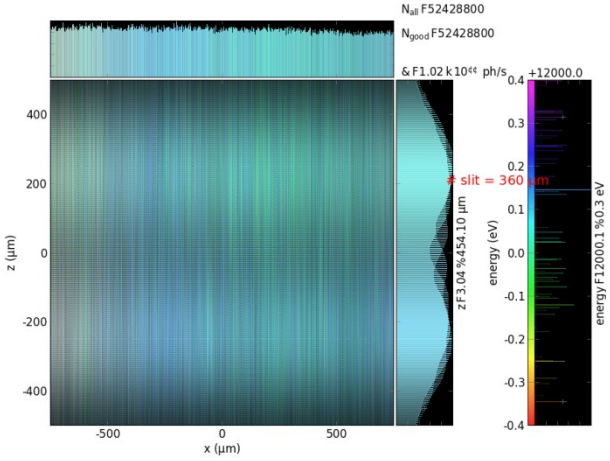
N_all F52428800
N_good F52428800
& F1.02 k10^6 ph/s
+12000.0
slit = 360 µm
z F3.04 %454.10 µm
energy (eV)
energy F12000.1 %0.3 eV
z (µm)
x (µm)

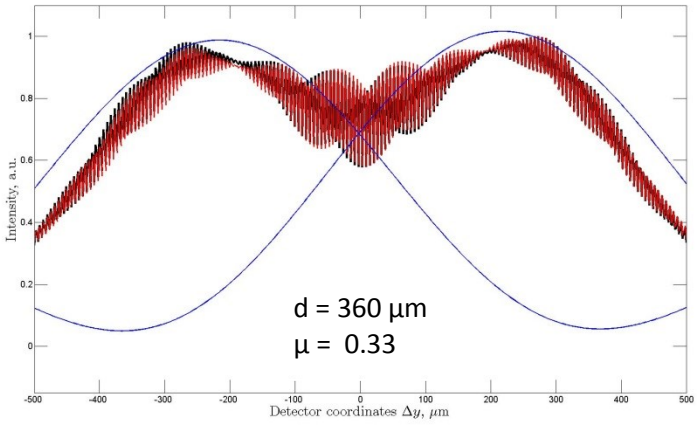
d = 360 µm
µ = 0.33
Intensity, a.u.
Detector coordinates Δy, µm

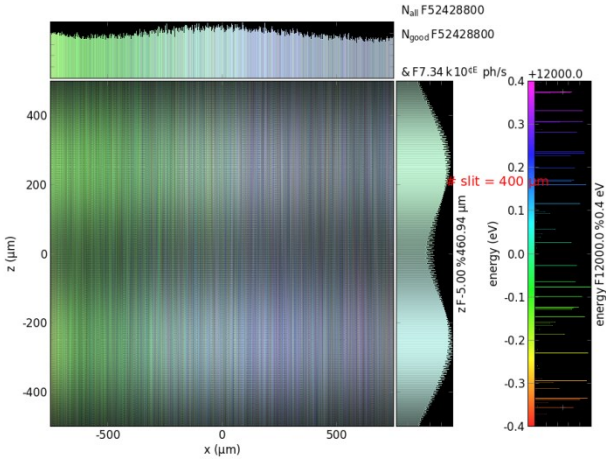
N_all F52428800
N_good F52428800
& F7.34 k10^6 ph/s
+12000.0
slit = 400 µm
z F-5.00 %460.94 µm
energy (eV)
energy F12000.0 %0.4 eV
z (µm)
x (µm)

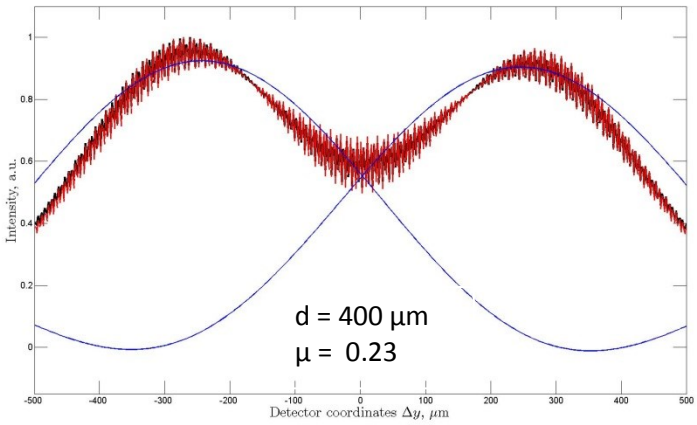
d = 400 µm
µ = 0.23
Intensity, a.u.
Detector coordinates Δy, µm